

Article

Comparison of Raman Spectra of Optically Nonlinear LiTaO₃:Cr³⁺ (0.005 wt%) Crystal Laser Excited in Visible (532 nm) and Near-IR (785 nm) Areas

Mikhail Palatnikov ^{1,*}, Nikolay Sidorov ¹, Alexander Pyatyshev ² and Alexander Skrabatun ²

¹ Tananaev Institute of Chemistry—Subdivision of the Federal Research Centre “Kola Science Centre of the Russian Academy of Sciences”, 184206 Apatity City, Russia; n.sidorov@ksc.ru

² P.N. Lebedev Physical Institute of the Russian Academy of Sciences, 119991 Moscow, Russia; jb_valensia@mail.ru (A.P.); skrabatunav@lebedev.ru (A.S.)

* Correspondence: m.palatnikov@ksc.ru

Abstract: Raman spectra have been excited by the radiation of lasers generating in the visible (532 nm) and near-IR (785 nm) ranges in a LiTaO₃:Cr³⁺ (0.005 wt%) crystal. The obtained spectra were compared. Recorded Raman spectra contained bands in the range of <900 cm⁻¹ (first order) up to 2000 cm⁻¹ (second order). The Raman spectra of the second order, excited by near-IR laser radiation, were located against the background of a wide, luminescent halo. The frequency of a single low-intensity band exceeded the exact frequency of an overtone corresponding to the completely symmetric fundamental 4A₁(z)LO mode. The attribution of other second-order bands with higher frequencies remains unclear.

Keywords: lithium tantalate; doping; transition element; ferroelectric; Raman scattering; second-order spectra; biphonon



Citation: Palatnikov, M.; Sidorov, N.; Pyatyshev, A.; Skrabatun, A. Comparison of Raman Spectra of Optically Nonlinear LiTaO₃:Cr³⁺ (0.005 wt%) Crystal Laser Excited in Visible (532 nm) and Near-IR (785 nm) Areas. *Photonics* **2023**, *10*, 439. <https://doi.org/10.3390/photonics10040439>

Received: 10 March 2023

Revised: 5 April 2023

Accepted: 11 April 2023

Published: 12 April 2023



Copyright: © 2023 by the authors. Licensee MDPI, Basel, Switzerland. This article is an open access article distributed under the terms and conditions of the Creative Commons Attribution (CC BY) license (<https://creativecommons.org/licenses/by/4.0/>).

1. Introduction

The ferroelectric single crystal of lithium tantalate (LT, LiTaO₃) has unique electro-optical, piezoelectric, pyroelectric and nonlinear optical characteristics. These properties make it a valuable and multifunctional material. The LiTaO₃ crystal is widely used to create IR radiation sensors, motion detectors and thermometry, as well as to generate terahertz radiation [1–7]. In addition, the development of materials based on a LT crystal for the purpose of converting and modulating optical radiation and for active nonlinear laser media is promising at present [8]. Lithium tantalate has classically been used as an active medium for parametric light generation [9–11]. For successful application, it is necessary to know the features of the interaction of radiation with different wavelengths and the active medium. In this regard, it seems relevant to study the interaction of lithium tantalate with laser radiation of various wavelengths.

LT is a nonstoichiometric oxygen octahedral phase of variable composition with a wide homogeneity region on the phase diagram [12]. This circumstance helps to continuously improve the technologies for growing single crystals with different Li/Ta ratios and to obtain materials with significantly better physical characteristics. These crystals can be nominally pure, i.e., the charge is not doped intentionally, but crystal contains a number of uncontrolled impurities in very small concentrations, or doped with a variety of elements. Features of the electrical and nonlinear optical characteristics of the LiTaO₃ crystal largely depend on the following factors: the polarizability of oxygen octahedral clusters MeO₆ (Me: Ta⁵⁺, Li⁺, dopant, impurity, vacancy V) by anharmonic interactions in the vibrations of ions and the magnitude of spontaneous polarization. Point defects are usually Me cations and V vacancies irregularly located along the polar axis of the crystal [8,12,13]. The defects play a significant role in clusters polarizability and spontaneous polarization.

When a developed functional non-linear optical material is proposed to convert IR radiation, it is necessary to minimize thermal and photo-induced (optical damage) variations in the refractive index. These changes distort the wavefront of the laser radiation propagation and significantly impair the operation of optoelectronic devices. Other distortions of the crystal structure are associated with its disordered and anharmonic structure; the structure is distorted due to compositional variability. It is widely known that Raman scattering reflects the slightest reordering of the crystal structural units [14–16]. Comparative studies are necessary for the creation of materials suitable for active nonlinear laser media, and to convert IR radiation into a visible form. Such studies can elucidate the differences between the passage of a visible laser and IR radiation through a photorefractive electro-optical crystal. The difference can be explained as follows: in micro- and macrostructures, point defects respond differently to exposure to different wavelengths. These point defects in photorefractive phases of variable composition are usually irregularly arranged main, doping (in case of doped crystals) and impurity atoms; such defects are the result of structural disorder and anharmonicity.

The optical properties of $\text{LiTaO}_3:\text{Cr}^{3+}$ crystals have been studied previously in a number of works [17–35]. According to these references, the absorption spectrum of $\text{LiTaO}_3:\text{Cr}^{3+}$ has two broad bands near 458.5 and 653 nm and a small maximum near 718.5 nm at room temperature. The two wide bands in the smaller wavelength area correspond to spin-allowed vibronic transitions ${}^4\text{A}_2\text{--}{}^4\text{T}_1$ and ${}^4\text{A}_2\text{--}{}^4\text{T}_2$. It is likely that a small maximum in the red region of the spectrum corresponds to the spin-forbidden zero-phonon transition ${}^2\text{E}\text{--}{}^4\text{A}_2$. The dependence of absorption on the concentration of chromium dopant was analyzed at a wavelength of 300 nm. The analysis showed that the absorption was negligible, with a chromium ion content less than 0.5 ppm. The luminescence spectrum at room temperature has a similar broad band; with a maximum at 858 nm, and shifted to 889 nm upon cooling to 5 K. This band corresponds to the ${}^4\text{T}_2\text{--}{}^4\text{A}_2$ vibronic transition. The dependence of polarized and unpolarized absorption and luminescence spectra on temperature (in the range of 5–390 K), pressure (up to 93 Kbar), and the lifetimes of luminescence centers were studied. A strong distortion of the beam profile of the 488 nm argon laser radiation transmitted through the $\text{LiTaO}_3:\text{Cr}^{3+}$ crystal was found. The distortion limits the application of this crystal as an active laser medium. Photoinduced and Rayleigh light scattering in a $\text{LiTaO}_3:\text{Cr}^{3+}$ crystal were analyzed in the works outlined in [34,35]. The isotropic nature of photoinduced light scattering was discovered, while the Rayleigh scattering of light had a nonstationary character. The $\text{LiTaO}_3:\text{Cr}^{3+}$ crystal was studied by nuclear and electron magnetic resonance in [36–42]. Unfortunately, data on the Raman spectra of both orders of $\text{LiTaO}_3:\text{Cr}^{3+}$ were absent from the cited works [17–42].

Comparative studies of the Raman spectra of a $\text{LiTaO}_3:\text{Cr}^{3+}$ (0.005 wt%) (LT:Cr) crystal recorded upon excitation by visible (532 nm) and near-IR (785 nm) laser radiation were performed in this work. Chromium in isomorphous LiTaO_3 and LiNbO_3 crystals has a constant valence (+3), and is not a photovoltaically active dopant. Its presence in the crystal structure does not increase the effect of photorefraction [14]. The valence (oxidation state of chromium) varies from +2 to +6 in other environments. Therefore, $\text{LiTaO}_3:\text{Cr}^{3+}$ crystals, as materials for nonlinearly active laser media, have a high resistance to the pump laser radiation. The concentration of the active Cr^{3+} ion in the crystal should be low enough so as not to increase the disorder and anharmonicity of the crystal lattice and not to deteriorate the optical quality of the crystal. The fact is that the Cr^{3+} ion in the cationic sublattice of LiTaO_3 and LiNbO_3 crystals can be in three positions [14]. The Cr^{3+} ion is localized in the vacant O_6 octahedron (Cr_V point defect) at low concentrations (≈ 0.005 wt% or less). If the concentration increases further, the Cr^{3+} ion additionally occupies lithium (Cr_{Li} point defect) and niobium octahedra (Cr_{Nb} point defect). Doping with Cr significantly decreases the cation sublattice order along the polar axis, and optical characteristics of the crystals deteriorate. Such disordering effects can manifest themselves in the spectra of second-order Raman scattering. Thus, the study of second-order Raman spectra can be an effective tool for the control of structure perfection of the crystal. Spectra of a perfect or near-ideal LT

crystal should not contain any bands in the second order range. As an LT crystal disorder grows, the anharmonism of the vibrations should increase; this should widen the first-order Raman bands and increase the intensity of the second-order bands. The changes in width and intensity should depend on the frequency of the exciting laser radiation and manifest themselves differently in the Raman spectrum when they are excited in the visible and IR regions.

2. Materials and Methods

This work considers the Raman spectra of a single LiTaO₃:Cr (0.005 wt%) crystal. Chromium Cr³⁺ is a photorefractive dopant that increases the sensitivity of the crystal to optical damage. A LiTaO₃:Cr (0.005 wt%) crystal was grown in an argon atmosphere using the Czochralski method from a Pt/Rh10 Ø 80 mm crucible, under conditions of an average axial gradient of ~10 deg/cm in the direction of the X-axis (X-cut) at a rotation speed of ~16 rpm and displacement of ~2.4 mm/h. The crystal growth rate was ~2.9–3.0 mm/h. Crystals were grown on a growth setup with an automatic crystal diameter control system. The features of single crystal growth were described in detail in [17,20]. The congruent melt ([Li]/[Ta] ≈ 0.92) was directly doped with chromium oxide (Cr₂O₃). The samples used to study the Raman spectra were cut from the grown boule in the shape of rectangular parallelepipeds. Their edges coincided with the directions of the main crystallophysical axes (x and y; z is the polar axis). The faces of the parallelepipeds were carefully polished.

Figure 1 shows a photograph of the test sample.

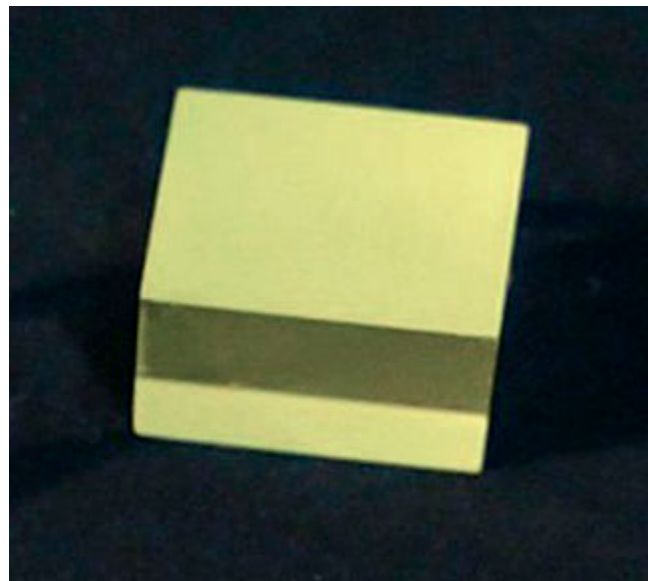


Figure 1. Photograph of a LiTaO₃:Cr (0.005 wt%) crystal sample.

Growth was completed when the weight of the LiTaO₃:Cr (0.005 wt%) crystal reached ~500 g. In this case, about ~28% of the total weight of the melt crystallized. The growth parameters of the LiTaO₃:Cr (0.005 wt%) crystal took into account the need to obtain a flat crystallization front. They were selected experimentally. The parameters were as follows: pulling speed, rod rotation speed and temperature gradient at the crystallization front. Such an approach should have provided a sufficiently high structural perfection of the crystal. The grown LiTaO₃:Cr (0.005 wt%) crystal had a flat crystallization front, Ø~38 mm, and the length of the cylindrical part was $L_c \approx 44$ mm. Dopant was introduced into the charge in the form of Cr₂O₃ (99.9) with a concentration of impurities at a level of $<3 \times 10^{-4}$ wt%. After addition, dopant was mixed thoroughly with the initial charge. The dopant was intended to homogenize in the melt. In order to achieve this goal, the melt was held for 9 h at the temperature ~90 °C higher than the LiTaO₃ melting point ($T_{\text{melt}} = 1650$ °C) before crystal growth.

The crystal was in a single-domain state. High-temperature electrodiffusion annealing was performed in LANTAN (Voroshilovgradsky zavod elektronnoy mashinostroeniya, Voroshilovgrad, USSR). The static piezoelectric effect controlled the degree of single-domain fraction [43]. The LiTaO₃:Cr (0.005 wt%) crystal was annealed at 1400 °C in a growth setup for 10 h and then cooled at a rate of ~50 K/h after growth. Prolonged post-growth annealing is required in order to homogenize the composition of the doped crystal and remove thermal and mechanical stresses.

Tantalum pentoxide Ta₂O₅, produced by Solikamsk magnesium works (Solikamsk, Russian Federation), and lithium carbonate Li₂CO₃ with an impurity concentration of $<3 \times 10^{-4}$ wt% were used to synthesize the LiTaO₃ charge.

A charge of congruent composition ([Li]/[Ta] \approx 0.92) was synthesized from these initial components. The impurity composition of the LiTaO₃ charge and the grown LiTaO₃:Cr (0.005 wt%) crystal determined by spectral analysis is shown in Table 1. As one can see from the table, the content of trace amounts of impurities in the crystal was no more than 10^{-4} wt%.

Table 1. Content of impurities in the charge and grown LiTaO₃:Cr (0.005 wt%) crystal.

Impurity	Concentration in the Charge, wt%	Concentration in LiTaO ₃ :Cr (0.005 wt%) Crystal, wt%
Mn, V, Mg, Sn	$<3 \times 10^{-4}$	$<1 \times 10^{-4}$
Pb, Ni	$<4 \times 10^{-4}$	$<2 \times 10^{-4}$
Co, Mo	$<4 \times 10^{-4}$	$<3 \times 10^{-4}$
Si, Fe	$<4 \times 10^{-4}$	$<4 \times 10^{-4}$
Ti	$<5 \times 10^{-4}$	$<5 \times 10^{-4}$
Al	$<6 \times 10^{-4}$	$<6 \times 10^{-4}$
Zr	$<7 \times 10^{-4}$	$<5 \times 10^{-4}$
Ca	$<3 \times 10^{-4}$	$<5 \times 10^{-4}$
Te, Sb	$<5 \times 10^{-4}$	$<4 \times 10^{-4}$
Bi	$<2 \times 10^{-4}$	$<2 \times 10^{-4}$
Rh	$<1 \times 10^{-4}$	$<2 \times 10^{-2}$

Raman spectra in the visible region were recorded by a BWS465-532S i-Raman Plus spectrometer (B&W Tek, Plainsboro Township, NJ, USA). The Raman setup contained a built-in cw laser with a 532 nm wavelength. This spectrometer is able to record spectra in the range of 50–4000 cm⁻¹. The laser power was 30 mW when the spectra were recorded in this setup. The numerical aperture of the objective of the Raman system was \approx 0.22. A BWS465-785H i-Raman Plus spectrometer (B&W Tek, Plainsboro Township, NJ, USA) was used to record Raman spectra in the near-IR region. It had a cw laser with excitation wavelength of 785 nm. This setup was able to record spectra in the range of 50–2850 cm⁻¹. The laser radiation power was 340 mW on the sample when the spectra were recorded in this setup. The numerical aperture of the objective of the Raman system was \approx 0.22. The laser spot size was 85 μ m at the focus in all experiments. Spectra, in both cases, were recorded in backscattering geometry at room temperature. The local influence of the exciting laser radiation was minimized, and the optimal radiation focus and accumulation time of the useful signal were adjusted for each experiment. The frequency error of the Raman bands was \pm 3.0 cm⁻¹.

3. Results and Discussion

The rhombohedral unit cell of the ferroelectric phase of the LiTaO₃ crystal is characterized by a C_{3v}⁶ space symmetry group (R3c). A LT unit cell contains two formula units made up of ten atoms. The lithium and tantalum atoms occupy the C₃ position. Oxygen atoms occupy the C₁ position. The curve of phonon dispersion has 30 vibrational branches; 27 of

them are optical and 3 are acoustic. The form of optical vibrational representation in LT can be expressed by the following equation:

$$\Gamma = 5A_1(z) + 5A_2 + 10E(x,y)$$

In this representation, $4A_1(z) + 9E(x,y)$ dipole active fundamental vibrations are active in Raman and IR absorption at $k = 0$ (i.e., at the center of the Brillouin zone). The polar nature of optical vibrations split them into longitudinal (LO) and transverse (TO) vibrations. Therefore, the Raman spectra should contain 26 bands attributed to fundamental phonons, given two conditions: phonons propagate along the crystallographic axes, and LO-TO split exists. In addition, $A_1(z) + E(x,y)$ acoustic and $5A_2$ optical fundamental vibrations are inactive. These bands are expected not to appear in either the Raman or the IR absorption spectra. The Raman tensor form [44] implies that (zz) polarization has only nondegenerate phonons of $A_1(z)$ symmetry, and (xy), (xz), (yx), (yz), (zx) and (zy) polarizations have only doubly degenerate $E(x,y)$ symmetry-type phonons. Both (xx) and (yy) polarizations should simultaneously have $A_1(z)$ and $E(x, y)$ symmetry-type phonons.

Figures 2 and 3 show the Raman spectra of a LT:Cr crystal recorded in $x(\bar{z}\bar{z}, \bar{z}\bar{y})\bar{x}$, $y(\bar{z}\bar{z}, \bar{z}\bar{x})\bar{y}$ and $z(\bar{x}\bar{x}, \bar{y}\bar{y}, \bar{x}\bar{y})\bar{z}$ scattering geometries excited by 532 and 785 nm laser radiation, respectively. Table 2 lists the frequencies of the experimentally observed bands in the Raman spectrum, corresponding to the fundamental vibrations of the crystal lattice and their attribution based on [44]. Table 2 also demonstrates alternative and ambiguous attributions (in brackets) for some of the Raman bands. According to [45], the 740 and 749 cm^{-1} bands can be attributed to LT intrinsic defects. Finally, the 717–721 and 810–812 cm^{-1} bands seem to correspond to two-phonon Raman processes.

Table 2. Real frequencies of polar vibrations (both transverse (TO) and longitudinal (LO)) of the LT:Cr crystal obtained in this study, and their attribution.

$\lambda_0 = 532 \text{ nm}$			$\lambda_0 = 785 \text{ nm}$			Attribution
ν, cm^{-1}						
$x(\bar{z}\bar{z}, \bar{z}\bar{y})\bar{x}$	$y(\bar{z}\bar{z}, \bar{z}\bar{x})\bar{y}$	$z(\bar{x}\bar{x}, \bar{y}\bar{y}, \bar{x}\bar{y})\bar{z}$	$x(\bar{z}\bar{z}, \bar{z}\bar{y})\bar{x}$	$y(\bar{z}\bar{z}, \bar{z}\bar{x})\bar{y}$	$z(\bar{x}\bar{x}, \bar{y}\bar{y}, \bar{x}\bar{y})\bar{z}$	
140	140	143	142	142	142	1E(x,y)TO
			190	190		1E(x,y)LO
203	203	206	207	207	207	1A ₁ (z)TO
		250	249	247		3E(x,y)TO
			279	277		3E(x,y)LO
312	312	309	314	314	314	4E(x,y)TO
356	353	356	356	356	354	2A ₁ (z)LO
377	380	377	380	380	381	3A ₁ (z)TO(5E(x,y)TO)
		403				3A ₁ (z)LO
458	458	461	462	463	463	7E(x,y)TO
595	595	592	596	599	594	4A ₁ (z)TO(8E(x,y)TO)
657	654	657	659	659	664	8E(x,y)LO(9E(x,y)TO)
864	867	867	870	869	865	4A ₁ (z)LO(9E(x,y)LO)

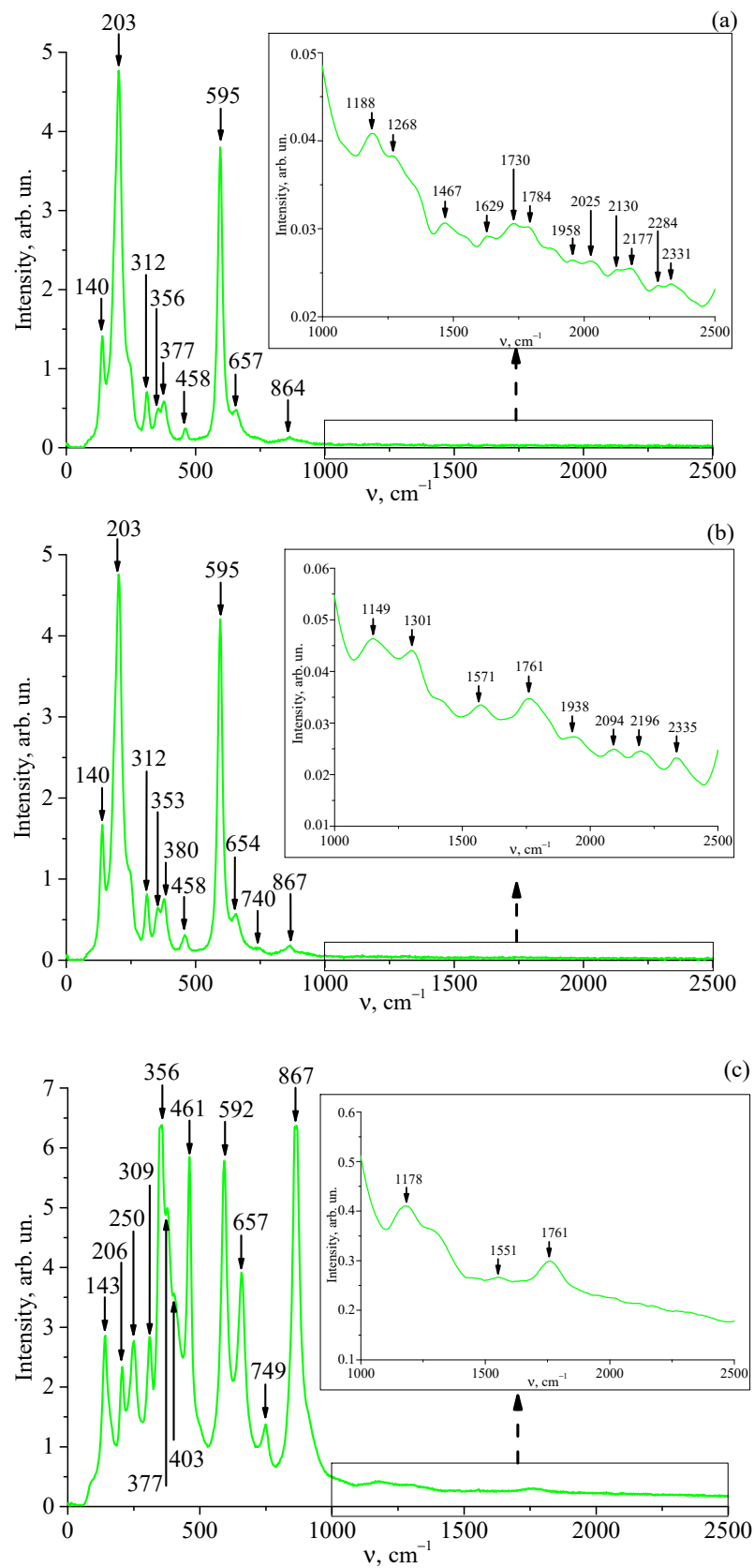


Figure 2. Raman spectra excited by $\lambda_0 = 532$ nm radiation in the LT:Cr crystal in $x(zz, zy) \bar{x}$ (a), $y(zz, zx) \bar{y}$ (b) and $z(xx, yy, xy) \bar{z}$ (c) scattering geometries.

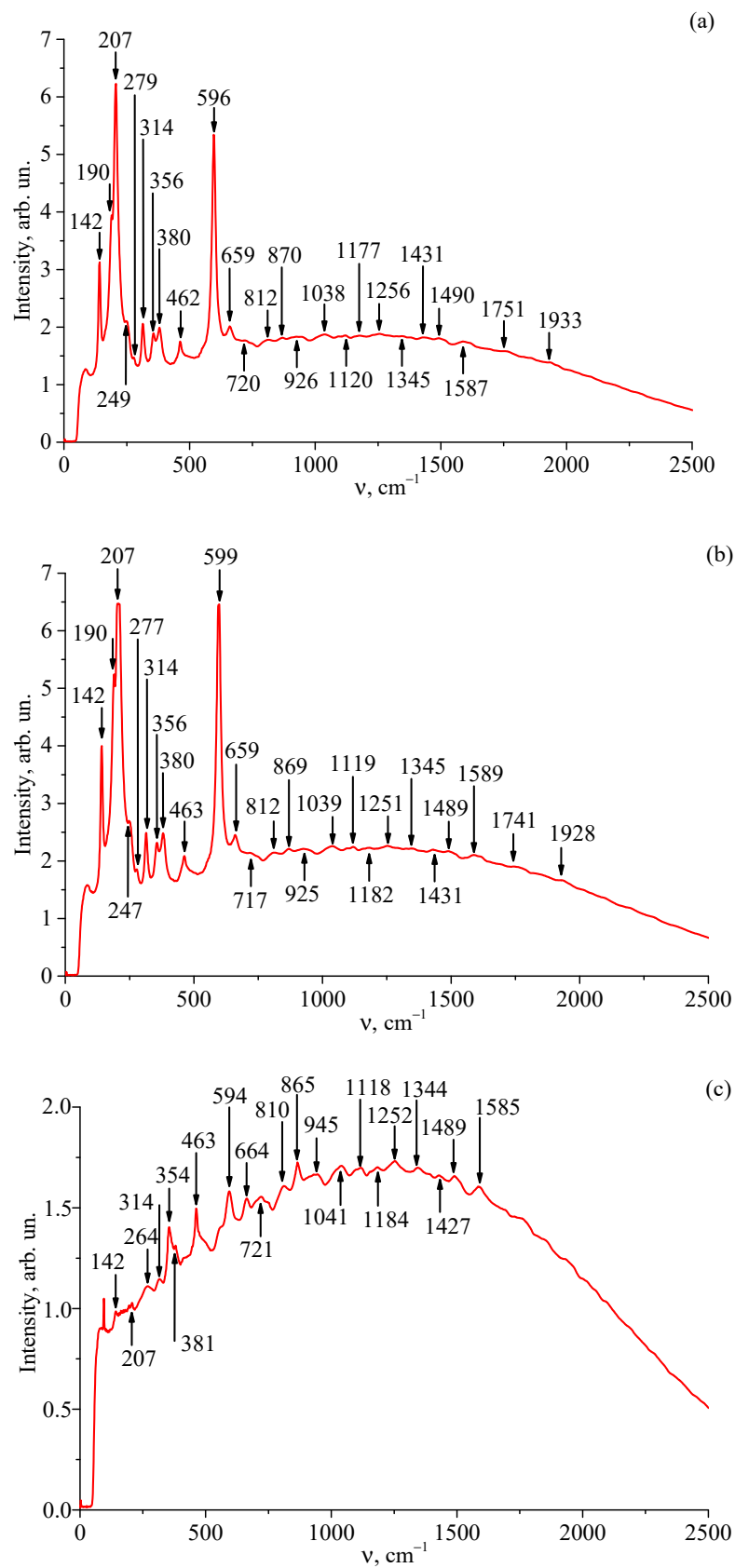


Figure 3. Raman spectra excited by $\lambda_0 = 785 \text{ nm}$ radiation in the LT:Cr crystal in scattering geometries $x(zz, zy) \bar{x}$ (a), $y(zz, zx) \bar{y}$ (b) and $z(xx, yy, xy) \bar{z}$ (c).

Our comparison of the data in Table 2 and Figures 2 and 3 revealed that the Raman spectra of the LT:Cr crystal significantly differed when excited by laser bands with frequencies of 532 and 785 nm. In addition, noticeable frequency differences for the TO and LO modes were observed. This indicates fundamental polar vibrations in noncentrosymmetric crystals. Figure 2 and Table 2 demonstrate that the fundamental vibrations bands were predominantly present upon excitation by 532 nm laser radiation in the Raman spectra of the crystal in the frequency range of 50–900 cm^{-1} . Additionally, bands with frequencies of 206–209, 250, 353–356 and 592–595 cm^{-1} were attributed to the $A_1(\text{TO})$ and $A_1(\text{LO})$ symmetry-type fundamental vibrations along the polar axis of the crystal, and bands with frequencies 377–380, 458–461, 654–657, 740–749 and 864–867 cm^{-1} were attributed to the fundamental doubly degenerate $E(\text{TO})$ and $E(\text{LO})$ symmetry-type vibrations perpendicular to the polar axis of the crystal. Figure 2 and Table 2 also show that unmixed (LO-TO) phonons could be observed in the spectrum of the LT:Cr crystal when it was excited by a 532 nm laser line. Mixed (LO-TO) phonons manifested in the spectrum when the phonon wave vector direction did not coincide with the direction of the main crystallographic axes. Furthermore, low-intensity extra bands were absent from the 50–900 cm^{-1} region of Raman spectrum of the LT:Cr crystal. According to selection rules for the space group $R3c$, these bands were not meant to appear, given that the unit cell contained two formula units. Low-intensity bands appeared in the spectrum of an isomorphous LiNbO_3 crystal of nonstoichiometric composition in the frequency range of 50–900 cm^{-1} due to the deviation of the crystal's composition from stoichiometric [14,46]. A number of broad low-intensity bands corresponding to the second-order Raman spectrum were present in the region of 900–2500 cm^{-1} . Some of the second-order bands were polarized. Bands appeared only in certain backscattering geometry. It is important to note that photoluminescence was absent in the entire studied frequency range of 50–2500 cm^{-1} when the Raman spectrum was excited by the 532 nm line. However, it has been observed prior, according to the data of [22–25], when the spectrum of a LT:Cr crystal was excited by the 640 nm band.

Figure 3 shows that the Raman spectrum excited by a 785 nm laser line was located against the background of an intense broad photoluminescence band with a maximum of $\approx 1250 \text{ cm}^{-1}$. The luminescent halo in the near IR region may be attributable to the luminescence centers in the LT:Cr crystal. The luminescence centers in the crystal are point defects of Cr_{Ta} and Cr_{Li} (Cr^{3+} ions located in the positions of tantalum and lithium ions). The luminescent halo can also be explained by defects in the form of small-radius polarons (Ta_{Li}) and more complex bipolaron bonds (in the form of $\text{Ta}_{\text{Li}}\text{-Ta}_{\text{Ta}}$). It was important that the Raman spectrum excited by the 785 nm laser line would contain more bands (extra bands) in the region of fundamental vibrations of the crystal lattice (50–900 cm^{-1}) than the selection rules allowed in the $x(\text{zz}, \text{zy}) \bar{x}$, $y(\text{zz}, \text{zx}) \bar{y}$ and $z(\text{xx}, \text{yy}, \text{xy}) \bar{z}$ scattering geometries. Selection rules have considered LO-TO splitting for the space group $R3c$ (C_{3V}^6) in cases in which the unit cell contains two formula units. Extra bands have a low intensity; their frequencies are 264, 717–721 and 810–812 cm^{-1} ; and they appear in various scattering geometries in the frequency range of fundamental vibrations (50–900 cm^{-1}) in the spectrum. Bands with frequencies of 925–926, 1038–1041, 1118–1120, 1182–1190, 1251–1256, 1344–1345, 1427, 1489, 1585–1587, 1741–1751 and 1928–1933 cm^{-1} belong to the second-order Raman spectrum; the bands often appear in the $>900 \text{ cm}^{-1}$ region of the LT Raman spectrum. These bands correspond to overtone processes; they can be attributed to bound states of optical phonons. In the case of LT:Cr, only one weak band, with a frequency of 1928–1933 cm^{-1} in scattering geometries $y(\text{zz}, \text{zx}) \bar{y}$ and $z(\text{xx}, \text{yy}, \text{xy}) \bar{z}$, showed an anomaly: its frequency was much higher than the exact value of the overtone frequency. The initial band was located near 864–870 cm^{-1} , and it corresponded to the symmetrical fundamental vibration of $4A_1(z)\text{LO}$ (Figures 2 and 3). The exact overtone frequency should be located near 1728–1740 cm^{-1} , but the real band is 200 cm^{-1} higher.

The nature of the Raman bands in the $>2000 \text{ cm}^{-1}$ range remains unclear and requires further research. Raman spectra of the studied LT:Cr crystal, when excited by radiation with different wavelengths, differed significantly from each other in the scattering geometry

$z(xx, yy, xy) \bar{z}$. There can be two reasons for the observed difference: different distribution of trivalent chromium dopant Cr^{3+} relative to the ferroelectric axis of the crystal, and different mechanisms of interaction of laser radiation with the LT:Cr crystal.

Figures 2 and 3 show that the intensity of the second-order Raman spectrum of the LT:Cr crystal was several orders of magnitude lower than the intensity of the fundamental vibrations. This might give rise to the idea that these weak bands are artifacts of the spectrometers. However, we are sure of the opposite. Previously, second-order Raman spectra were studied in a number of crystals: diamond [47], gallium phosphide [48], cesium bromide [49], α -sulfur, etc. For example, the peak intensity of a number of lines in the diamond second-order Raman spectrum was from 250 to 10^5 times less than the intensity of the fundamental mode. The results of other works have stated that the second-order Raman spectrum has a quasi-continuous form, with weak maxima. In addition, in our previous works, we have studied lithium niobate and tantalate crystals with other dopants, and the second-order Raman spectrum had quite a low intensity [50–53]. Thus, it is not entirely correct to state that the weak bands in the $900\text{--}2000\text{ cm}^{-1}$ region are an artifact of the spectrometers used.

Thus, the LT:Cr Raman spectra excited by 532 and 785 nm laser radiation were found to be different. This difference can be explained as follows. The mechanisms of interaction between the visible and near-IR radiation and the microstructure and structural defects of the crystal are different. In addition, microstructures, together with defects, determine the bound states of phonons (i.e., phonon–phonon interaction) and, thus, the anharmonicity of the crystal lattice vibrations. The formation of bound states of phonons in crystals was schematically given in theoretical works [54–56]. These works showed that one-phonon Green’s function $D_1(k, \omega)$ can be used to calculate the density of two-phonon states $\rho_2(\omega)$ by employing five Formulas (1)–(5):

$$D_1\left(\vec{k}, \omega\right) = \frac{\omega\left(\vec{k}\right)}{2} \left[\frac{1}{\omega - \omega\left(\vec{k}\right) + \frac{1}{2}i\Gamma} - \frac{1}{\omega + \omega\left(\vec{k}\right) - \frac{1}{2}i\Gamma} \right] \tag{1}$$

$$F(\omega) = \frac{i}{(2\pi)^4} \int d^3 \vec{k} \int D_1\left(\vec{k}, \omega - \omega'\right) D_1\left(\vec{k}, \omega\right) d\omega' \tag{2}$$

The relation in (3) is correct for optical phonons with frequency ω_0 near the center of the Brillouin zone in the quasi-Newtonian approximation of the dispersion law for the density of single-particle states of phonons $\rho_1(\omega)$:

$$\rho_1(\omega) = a \sqrt{\omega_0 - \omega} \tag{3}$$

where $a = -\frac{\omega_0 V \sqrt{2\omega_0}}{2\pi^2 s^3}$, V denotes the unit cell volume and s is the speed of sound. As a result, the function $F(\omega)$ has the shape:

$$F(\omega) = \frac{1}{4} \omega_0^2 a \int_0^\Delta \frac{\sqrt{\omega'}}{\omega - 2(\omega_0 - \omega') + i\Gamma} d\omega' \tag{4}$$

where Δ is the range of phonon frequencies considered during the integration. The function $F(\omega)$ depends on two factors: the effective mass of the quasiparticle and the damping constant Γ . The constant can be associated with the inverse lifetime of the quasiparticle $\tau = 1/\Gamma$. The intensity of second-order Raman bands should then be proportional to the density of two-phonon states $\rho_2(\omega)$:

$$\rho_2(k, \omega) \approx -\frac{2}{\pi \omega_0^2} \frac{\text{Im } F(\omega)}{\left[1 - \frac{1}{2}g_4 \text{Re } F(\omega)\right]^2 + \left[\frac{1}{2}g_4 \text{Im } F(\omega)\right]^2} \tag{5}$$

Figure 4 compares theoretical calculations of the spectral distribution of the Raman intensity in the overtone region of $2\nu_0 = 1738 \text{ cm}^{-1}$, as well as the experimentally observed intensity distribution. The dotted arrow in Figure 4 locates the exact position of the $2\nu_0$ overtone.

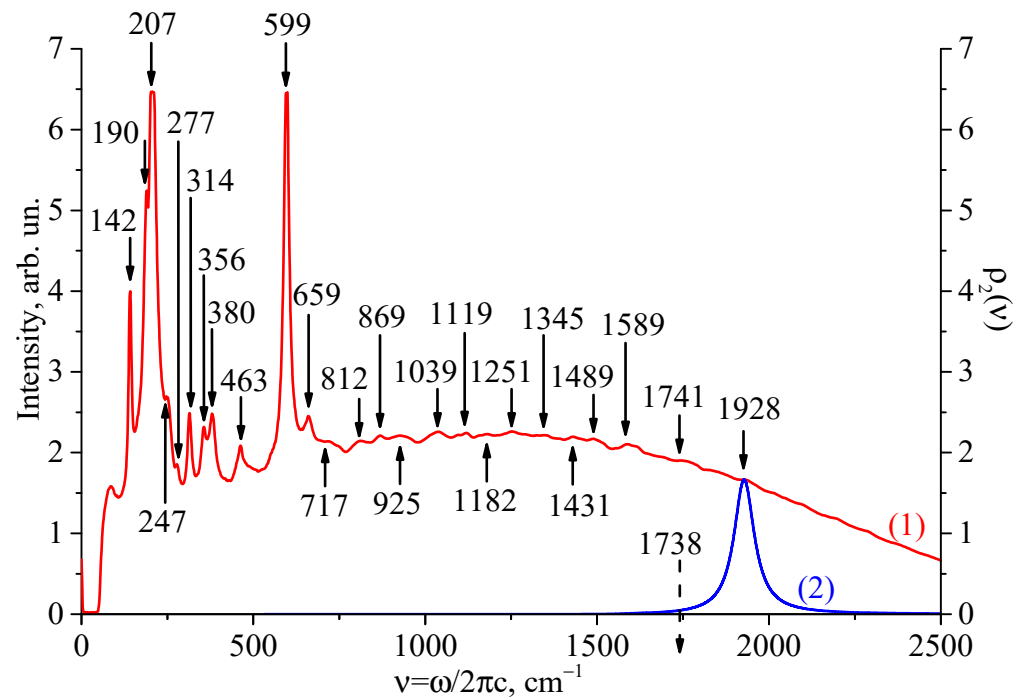


Figure 4. Comparison of the real Raman spectrum of the LT:Cr crystal (curve 1) with the calculated dependence of the two-phonon state density $\rho_2(\nu)$ in the overtone region (curve 2).

Figure 4 shows the bound state of the fully symmetric polar mode $4A_1(z)$ LO with a frequency of 869 cm^{-1} , satisfactorily approximating the 1928 cm^{-1} band (curve 2) at the following parameters: $s = 1000$, $\Delta = 0.1\omega_0$, $g_4 = 7.28 \times 10^{-18}$ and $\Gamma = 7.54 \times 10^{12}$. The Δ value was given by the dispersion curve form characteristic of optical phonons $4A_1(z)$. The damping constant Γ was equal to the width of the real Raman bands of these phonons.

4. Conclusions

In the present work, the full Raman spectra of a $\text{LiTaO}_3:\text{Cr}^{3+}$ (0.005 wt%) crystal with backscattering geometry in the frequency range of $50\text{--}2500 \text{ cm}^{-1}$ upon excitation by the 532 and 785 nm laser lines were recorded, and their interpretation was given. For the first time, the second-order Raman spectrum of a $\text{LiTaO}_3:\text{Cr}^{3+}$ (0.005 wt%) crystal was reported. This spectrum had weak bands in the range of $800\text{--}2000 \text{ cm}^{-1}$. Bands corresponded to overtone processes. A weak band with a maximum near 1928 cm^{-1} was found among these bands in the Raman spectrum. Its frequency value exceeded the exact value of the overtone of the symmetric fundamental mode $4A_1(z)$.

Comprehensive studies on nonlinear optical processes in this crystal are of interest for future studies. By nonlinear processes, we mean, for example, stimulated Raman scattering of light, generation of the second optical harmonic, generation of sum and difference optical harmonics and parametric generation of light. Since Cr^{3+} chromium ions exhibit intense luminescence in the near-IR region, the $\text{LiTaO}_3:\text{Cr}^{3+}$ (0.005 wt%) crystal studied in this work may be used as an active laser medium in the future. However, for this purpose, it is necessary to grow a crystal with a much more perfect structure. It is also necessary to establish and study the optimization of the conditions in order to observe laser generation in this crystal.

Author Contributions: Conceptualization, N.S.; validation, N.S.; investigation, A.P. and A.S.; data curation, A.P. and A.S.; writing—original draft preparation, N.S. and A.P.; writing—review and editing, M.P.; visualization, M.P. and A.S.; supervision, M.P. All authors have read and agreed to the published version of the manuscript.

Funding: This work was supported by the Ministry of Higher Education, Russian Federation, scientific topics 0186-2022-0002 (registration FMEZ-2022-0016) and the joint Russian Foundation for Basic Research and Belarus Foundation for Basic Research grant 20-52-04001 Bel_mol_a.

Institutional Review Board Statement: Not applicable.

Informed Consent Statement: Not applicable.

Data Availability Statement: The data obtained in this research will be available from the corresponding author, M.P., upon reasonable request.

Conflicts of Interest: The authors declare no conflict of interest.

References

- Blázquez-Castro, A.; García-Cabañes, A.; Carrascosa, M. Biological applications of ferroelectric materials. *Appl. Phys. Rev.* **2018**, *5*, 041101. [\[CrossRef\]](#)
- Irzaman; Siskandar, R.; Nabilah, N.; Aminullah; Yuliarto, B.; Haman, K.A.; Husin, A. Application of lithium tantalate (LiTaO₃) films as light sensor to monitor the light status in the Arduino Uno based energy-saving automatic light prototype and passive infrared sensor. *Ferroelectrics* **2018**, *524*, 44–55. [\[CrossRef\]](#)
- Yang, X.; Lin, S.; Ma, D.; Long, S.; Zhu, Y.; Li, H.; Wang, B. Up-conversion luminescence of LiTaO₃:Er³⁺ phosphors for optical thermometry. *Ceram. Intern.* **2020**, *46*, 1178–1182. [\[CrossRef\]](#)
- Yao, S.; Han, H.; Jiang, S.; Xiang, B.; Chai, G.; Ruan, S. Design, simulation, and analysis of optical microring resonators in lithium tantalate on insulator. *Crystals* **2021**, *11*, 480. [\[CrossRef\]](#)
- He, Y.; Wong, Y.P.; Liang, Q.; Wu, T.; Bao, J.; Hashimoto, K.Y. Transverse energy confinement and resonance suppression in SAW resonators using low-cut lithium tantalate. *Jap. J. Appl. Phys.* **2022**, *61*, SG1031. [\[CrossRef\]](#)
- Wu, B.; Zhang, B.; Liu, W.; Lu, Q.; Wang, L.; Chen, F. Recoverable and rewritable waveguide beam splitters fabricated by tailored femtosecond laser writing of lithium tantalate crystal. *Opt. Laser Technol.* **2022**, *145*, 107500. [\[CrossRef\]](#)
- Lyu, T.; Dorenbos, P.; Xiong, P.; Wei, Z. LiTaO₃:Bi³⁺, Tb³⁺, Ga³⁺, Ge⁴⁺: A smart perovskite with high charge carrier storage capacity for X-ray imaging, stress sensing, and non-real-time recording. *Adv. Funct. Mater.* **2022**, *32*, 2206024. [\[CrossRef\]](#)
- Sidorov, N.V.; Palatnikov, M.N.; Biryukova, I.V.; Titov, R.A.; Makarova, O.V.; Masloboeva, S.M. *Monocrystals of Lithium Niobate and Tantalate of Different Composition and Genesis*; RAN: Moscow, Russia, 2022; 288p. (In Russian)
- Chuchumishev, D.; Gaydardzhiev, A.; Fiebig, T.; Buchvarov, I. Subnanosecond, mid-IR, 0.5 kHz periodically poled stoichiometric LiTaO₃ optical parametric oscillator with over 1 W average power. *Opt. Lett.* **2013**, *38*, 3347–3349. [\[CrossRef\]](#)
- Yin, M. Broadband quasi-phase-matching second-harmonic generation in 0.5 mol% MgO-doped periodically poled stoichiometric LiTaO₃. *J. Korean Phys. Soc.* **2015**, *67*, 1750–1754. [\[CrossRef\]](#)
- Chuchumishev, D.; Trifonov, A.; Oreshkov, B.; Xu, X.; Buchvarov, I. High-energy picosecond kHz optical parametric oscillator/amplifier tunable between 3 and 3.5 μm. *Appl. Phys. B* **2018**, *124*, 1–6. [\[CrossRef\]](#)
- Prokhorov, A.M.; Kuz'minov, Y.S. *Physics and Chemistry of Crystalline Lithium Niobate*; Adam Hilger: New York, NY, USA, 1990; p. 237.
- Huband, S.; Keeble, D.S.; Zhang, N.; Glazer, A.M.; Bartaszyte, A.; Thomas, P.A. Relationship between the structure and optical properties of lithium tantalate at the zero-birefringence point. *J. Appl. Phys.* **2017**, *121*, 024102. [\[CrossRef\]](#)
- Sidorov, N.V.; Volk, T.R.; Mavrin, B.N.; Kalinnikov, V.T. *Lithium Niobate: Defects, Photorefraction, Vibrational Spectrum, Polaritons*; Nauka: Moscow, Russia, 2003; p. 255. (In Russian)
- Fontana, M.D.; Bourson, P. Microstructure and defects probed by Raman spectroscopy in lithium niobate crystals and devices. *Appl. Phys. Rev.* **2015**, *2*, 040602. [\[CrossRef\]](#)
- Wu, X.-L.; Yany, F.; Zhangy, M.-S.; Jiangy, S.-S.; Fengy, D. The microstructural difference between proton-exchanged LiNbO₃ and LiTaO₃ crystals by Raman spectroscopy. *J. Phys. Condens. Matter* **1996**, *8*, 2073–2080. [\[CrossRef\]](#)
- Glass, A.M. Optical spectra of Cr³⁺ impurity ions in ferroelectric LiNbO₃ and LiTaO₃. *J. Chem. Phys.* **1969**, *50*, 1501–1510. [\[CrossRef\]](#)
- Tsuya, H. Optical damage in transition-metal-doped LiTaO₃. *J. Appl. Phys.* **1975**, *46*, 4323–4333. [\[CrossRef\]](#)
- von der Linde, D.; Glass, A.M.; Rodgers, K.F. Optical storage using refractive index changes induced by two-step excitation. *J. Appl. Phys.* **1976**, *47*, 217–220. [\[CrossRef\]](#)
- Ryba-Romanowski, W.; Golab, S.; Pisarski, W.A.; Dominiak-Dzik, G.; Palatnikov, M.N.; Sidorov, N.V.; Kalinnikov, V.T. Influence of temperature on the optical properties of LiTaO₃:Cr. *Appl. Phys. Lett.* **1997**, *70*, 2505–2507. [\[CrossRef\]](#)
- Sokolska, I.; Golab, S.; Ryba-Romanowski, W. Optical spectroscopy of doped LiTaO₃ crystals. *Spectrochim. Acta Part A Mol. Biomol. Spectrosc.* **1998**, *54*, 1685–1694. [\[CrossRef\]](#)

22. Sokolska, I.; Kuck, S. Optical characterization of Cr³⁺ doped LiTaO₃ crystals relevant for laser application. *Spectrochim. Acta Part A Mol. Biomol. Spectrosc.* **1998**, *54*, 1695–1700. [[CrossRef](#)]
23. Golab, S.; Sokolska, I.; Dominiak-Dzik, G.; Palatnikov, M.N.; Sidorov, N.V.; Biryukova, I.; Kalinnikov, V.T.; Ryba-Romanowski, W. Optical absorption and luminescence of LiTaO₃:Cr and LiTaO₃:Cr,Nd crystals. *Proc. SPIE* **1999**, *3724*, 270–273. [[CrossRef](#)]
24. Alexandrovski, A.L.; Foulon, G.; Myers, L.E.; Route, R.K.; Fejer, M.M. UV and visible absorption in LiTaO₃. *Proc. SPIE* **1999**, *3610*, 44–51. [[CrossRef](#)]
25. Grinberg, M.; Sokolska, I.; Kuck, S.; Jaskolski, W. Temperature dependence of the luminescence decay of Cr³⁺ ions in LiTaO₃: Confined potential model. *Phys. Rev. B* **1999**, *60*, 959–965. [[CrossRef](#)]
26. Shen, Y.; Bray, K.L.; Grinberg, M.; Barzowska, J.; Sokolska, I. Identification of multisite behavior in a broadly emitting transition-metal system using pressure. *Phys. Rev. B* **2000**, *61*, 14263–14266. [[CrossRef](#)]
27. Shen, Y.; Bray, K.L.; Grinberg, M.; Barzowska, J.; Sokolska, I. High pressure spectroscopy of chromium doped LiTaO₃ crystals. *High Press. Res.* **2000**, *18*, 125–130. [[CrossRef](#)]
28. Kaczmarek, S.; Swirkowicz, M.; Jablonski, R.; Lukasiewicz, T.; Kwasny, M. Growth and characterization of lithium tantalate single crystals doped with Ho, Tm, Nd, Yb, Pr and doped by diffusion with Cr and Cu. *J. Alloys Compd.* **2000**, *300–301*, 322–328. [[CrossRef](#)]
29. Grinberg, M.; Barzowska, J.; Shen, Y.; Bray, K. Crystal field model of the three principal Cr³⁺ centers in LiTaO₃. *Radiat. Eff. Defects Solids* **2001**, *155*, 247–251. [[CrossRef](#)]
30. Grinberg, M.; Barzowska, J.; Bray, K.L.; Shen, Y.R. Inhomogeneous broadening of the dominant Cr³⁺ sites in LiTaO₃ system. *J. Luminesc.* **2001**, *94–95*, 85–90. [[CrossRef](#)]
31. Grinberg, M.; Barzowska, J.; Shen, Y.R.; Bray, K.L. Inhomogeneous broadening of Cr³⁺ luminescence in doped LiTaO₃. *Phys. Rev. B* **2001**, *63*, 214104. [[CrossRef](#)]
32. Grinberg, M. Spectroscopic characterisation of disordered materials doped with chromium. *Opt. Mater.* **2002**, *19*, 37–45. [[CrossRef](#)]
33. Grinberg, M.; Suchocki, A. Pressure-induced changes in the energetic structure of the 3d³ ions in solid matrices. *J. Luminesc.* **2007**, *125*, 97–103. [[CrossRef](#)]
34. Bagdasarov, K.S.; Batoev, V.B.; Uyukin, E.M. Transient isotropic photoinduced scattering of light in LiTaO₃:Cr. *Sov. J. Quant. Electron.* **1986**, *16*, 1295–1296. [[CrossRef](#)]
35. Batoev, V.B.; Uyukin, E.M. Photoinduced and Rayleigh light scattering in LiTaO₃:Cr. *Fiz. Tverd. Tela* **1988**, *30*, 1913–1915.
36. Burns, G.; O’kane, D.F. Optical and electron-spin-resonance spectra of Yb³⁺, Nd³⁺, and Cr³⁺ in LiNbO₃ and LiTaO₃. *Phys. Rev.* **1968**, *167*, 314–319. [[CrossRef](#)]
37. Chen, C.Y.; Sweeney, K.L.; Halliburton, L.E. Reduction and radiation effects in lithium tantalate. *Phys. Status Solidi* **1984**, *81*, 253–257. [[CrossRef](#)]
38. Ahn, S.W.; Kim, J.S.; Choh, S.H.; Yeom, T.H. An induced Cr³⁺ center in γ -irradiated LiTaO₃. *J. Kor. Phys. Soc.* **1994**, *27*, 535–537.
39. Ahn, S.W.; Rudowicz, C.; Choh, S.H.; Han, S.Y. EPR study of two Cr³⁺ defect centers in LiTaO₃ single crystals. *J. Korean Phys. Soc.* **1997**, *30*, 99–102.
40. Yeom, T.H.; Choh, S.H. Magnetic resonance investigations of LiNbO₃ and LiTaO₃ single crystals. *J. Korean Phys. Soc.* **1998**, *32*, S672–S675.
41. Loyo-Menoyo, M.; Keeble, D.J.; Furukawa, Y.; Kitamura, K. Electron paramagnetic resonance of Cr³⁺ in near-stoichiometric LiTaO₃. *J. Appl. Phys.* **2005**, *97*, 123905. [[CrossRef](#)]
42. Zhang, C.-X.; Kuang, X.-Y.; Mao, A.-J.; Wang, H. Optical spectrum, local lattice structure and EPR g factors for Cr³⁺ impurity ions in MgTiO₃ and LiTaO₃. *Phys. B Condens. Matter* **2008**, *403*, 3114–3118. [[CrossRef](#)]
43. Palatnikov, M.N.; Sandler, V.A.; Sidorov, N.V.; Efremov, I.N.; Makarova, O.V. Methods for controlling the degree of unipolarity of large LiNbO₃ crystals. *Instrum. Exp. Tech.* **2020**, *63*, 383–387. [[CrossRef](#)]
44. Sanna, S.; Neufeld, S.; Rusing, M.; Berth, G.; Zrenner, A.; Schmidt, W.G. Raman scattering efficiency in LiTaO₃ and LiNbO₃ crystals. *Phys. Rev. B* **2015**, *91*, 224302. [[CrossRef](#)]
45. Shi, L.; Kong, Y.; Yan, W.; Liu, H.; Li, X.; Xie, X.; Zhao, D.; Sun, L.; Xu, J.; Sun, J.; et al. The composition dependence and new assignment of the Raman spectrum in lithium tantalate. *Solid State Commun.* **2005**, *135*, 251–256. [[CrossRef](#)]
46. Sidorov, N.V.; Palatnikov, M.N. Raman spectra of lithium niobate crystals heavily doped with zinc and magnesium. *Opt. Spectrosc.* **2016**, *121*, 842–850. [[CrossRef](#)]
47. Solin, S.A.; Ramdas, A.K. Raman spectrum of diamond. *Phys. Rev. B* **1970**, *1*, 1687–1698. [[CrossRef](#)]
48. Sushchinsky, M.M.; Gorelik, V.S.; Maximov, O.P. Higher-order Raman spectra of GaP. *J. Raman Spectrosc.* **1978**, *7*, 26–30. [[CrossRef](#)]
49. Narayanan, P.S. Raman spectrum of cesium bromide. *Proc. Indian Acad. Sci. A* **1955**, *42*, 303–308. [[CrossRef](#)]
50. Sidorov, N.; Palatnikov, M.; Pyatyshev, A.; Sverbil, P. Second-order Raman scattering in ferroelectric ceramic solid solutions LiNb_xTa_{1-x}O₃. *Crystals* **2022**, *12*, 456. [[CrossRef](#)]
51. Sidorov, N.; Palatnikov, M.; Pyatyshev, A.; Skrabatun, A. Investigation of the structural perfection of a LiNbO₃:Gd³⁺(0.003):Mg²⁺(0.65 wt.%) double-doped single crystal using the Raman spectra excited by laser lines in the visible (532 nm) and near-IR (785 nm) regions. *Appl. Sci.* **2023**, *13*, 2348. [[CrossRef](#)]
52. Gorelik, V.S.; Abdurakhmonov, S.D. Overtone Raman scattering in lithium niobate single crystals doped with terbium. *Crystallogr. Rep.* **2022**, *67*, 252–255. [[CrossRef](#)]

53. Sidorov, N.; Palatnikov, M.; Pyatyshev, A. Raman scattering in a double-doped single crystal LiTaO₃:Cr(0.2):Nd(0.45 wt%). *Photonics* **2022**, *9*, 712. [[CrossRef](#)]
54. Ruvalds, J.; Zawadowski, A. Two-phonon resonances and hybridization of the resonance with single-phonon states. *Phys. Rev. B* **1970**, *2*, 1172–1175. [[CrossRef](#)]
55. Zawadowski, A.; Ruvalds, J. Indirect coupling and antiresonance of two optic phonons. *Phys. Rev. Lett.* **1970**, *24*, 1111–1114. [[CrossRef](#)]
56. Ruvalds, J.; Zawadowski, A. Resonances of two phonons from different dispersion branches. *Solid State Commun.* **1971**, *9*, 129–132. [[CrossRef](#)]

Disclaimer/Publisher’s Note: The statements, opinions and data contained in all publications are solely those of the individual author(s) and contributor(s) and not of MDPI and/or the editor(s). MDPI and/or the editor(s) disclaim responsibility for any injury to people or property resulting from any ideas, methods, instructions or products referred to in the content.